J Seismol (2012) 16:603–621
DOI 10.1007/s10950-012-9274-y

ORIGINAL ARTICLE

Rotaphone, a mechanical seismic sensor system for field rotation rate measurements and its in situ calibration

Johana Brokešová · Jiří Málek · Petr Kolínský

Received: 11 July 2011 / Accepted: 5 January 2012 / Published online: 24 February 2012

Abstract A newly developed mechanical sensor system, called a Rotaphone, for recording rotation rate components is described. The sensor system is based on measurements of the differential motions between paired low-frequency geophones attached to a rigid skeleton. The same differential velocity (and, consequently, the same rotation rate component) is obtained from more than one geophone pair, which allows for in situ calibration and matching of the individual sensors. The calibration method, which is a key point of our methodology, is explained in detail and demonstrated on synthetic examples. The instrument and the calibration technique were also subjected to laboratory testing utilizing a rotational shaking table. Some results of these tests are presented in comparison to the data from a reference sensor (fiber optic gyroscope). The new rotational seismic sensor system is characterized by a flat frequency response over a wide range from 2 to 200 Hz and sensitivity limit of the order of 10^{-8} rad/s. Its advantages are small size, portability, and easy installation and operation in the field. We present several examples of the vertical rotation rate ground motion recorded at Nový Kostel station (Czech Republic): first, a group of records of local micro-earthquakes which occurred in West Bohemia/Vogtland in May 2010 and, second, a record due to an anthropogenic source, a quarry blast at the nearby Vintířov quarry recorded in June 2010. The measured rotation rates are of order between 10^{-6} for the local earthquakes and 10^{-7} rad/s for the blast. These measurements demonstrate that the instrument has much wider application than just prospecting measurements, for which it was originally designed.

Keywords Seismic rotation · Rotational seismometer · Inverse problem · West Bohemia/Vogtland region

J. Brokešová (✉)
Department of Geophysics, Faculty of Mathematics and Physics, Charles University, V Holešovičkách 2, 180 00 Prague, Czech Republic
e-mail: Johana.Brokesova@mff.cuni.cz

J. Málek · P. Kolínský
Institute of Rock Structure and Mechanics, Academy of Sciences of the Czech Republic, V Holešovičkách 41, 182 09 Prague, Czech Republic

1 Introduction

Rotational seismology is an expanding seismological discipline, which has been emerging in the past decade and is attracting attention throughout the seismological community (Teisseyre et al. 2006). The basic source of information in rotational seismology is the measurement of seismic rotations or rotation rates. At present, various types of seismic rotational sensors are producing numerous rotational records for a wide range of epicentral distances. Rotational signals are detected from teleseismic (Igel et al. 2005), regional (Huang 2003), as well as local events (Nigbor 1994; Takeo 1998; Lee et al. 2009; Lin et al. 2009).

Several methodologies are used to measure seismic rotations. The most sensitive rotation data obtained up to now have been made by large ring laser gyroscopes (Stedman 1997; Schreiber et al. 2003, 2004, 2009). These gyroscopes utilize the Doppler frequency shift affecting the interference between two laser beams of the same constant wavelength propagating in opposite directions along a square or triangular perimeter due to a suitable mirror arrangement. The best reported ring laser sensitivity in measuring the seismic rotation rate is 10^{-12} rad/s (Schreiber et al. 2009). These instruments are useful in obtaining rotation rate records of teleseismic events. Their main disadvantages are high costs and special installation and maintenance requirements. They cannot be used for field measurements.

The urgent need for portable rotational sensors, easily installed and operated in the field, led to the development of various small mechanical, electrochemical, or fibre-optical rotational sensors. As far as the authors know, the only apropos small, portable seismic rotational sensor produced on a commercial basis are the R1 and R2 by Eentec, sensitivity of the former is reported to be 10^{-7} rad/s (Nigbor et al. 2009), and ARS-14 by Applied Technology Associates with the sensitivity 10^{-6} rad/s is reported by the contriver. In this paper, we briefly describe the newly developed rotational sensor system, the so-called Rotaphone, which also falls into the category of small, sensitive, portable rotational sensors useful for field measurements of local micro-earthquakes, rockbursts, and blasts. Its principle is, to some extent, similar to the device reported by Moriya and Teisseyre (2006), namely as to measuring finite ground motion spatial differences. An important advantage of our device over that effort and our earlier work is its increased sensitivity. That sensitivity depends on specific design features and the components used, but for prototypes tested to date, the sensitivity limit is estimated as 10^{-8} rad/s. For details, see the paper by Brokešová and Málek (2010). Measurement of self noise have not yet been performed.

In our method, the rotation measurement is based on approximating the spatial ground-motion derivatives through corresponding finite differences. This task requires measuring the differential motions, differences in the recordings from two sensors situated close to each other. The rotation measurement using small-aperture arrays (e.g., Huang 2003) is based on a similar idea. However, there are several differences between the two approaches. First, the distance between the individual sensors in the small-aperture arrays is usually several tens to several hundreds of meters, i.e., larger by several orders than in our case (~0.3 m). This causes many specific problems in deriving rotations, including different site conditions beneath the individual seismographs in the array. Second, the sensors in the small-aperture arrays operate independently of each other, and there is no rigid connection between them, so that their motion is determined not only by seismic translation and rotation but also by deformation of the ground in the array area.

The main factor limiting the accuracy of differential seismic motion measurements is the fact that the sensors used to derive the motion difference are not identical in terms of their transfer functions. This means that for the same input, they do not produce the same output. Even though the sensors used for this purpose are selected to be as similar as possible (same type, same manufacturer, etc.), small differences in their characteristics usually remain, causing contingent small relative errors in their recordings. Therefore, much attention should be paid to proper calibration of the individual sensors. In this paper, our in situ calibration technique is explained in detail and demonstrated on numerical examples.

The Rotaphone described in this paper was originally developed to operate with anthropogenic sources, namely a generator of rotational ground motion (Brokešová et al. 2009a), in prospecting measurements. However, when properly calibrated, it is capable of recording the seismic rotation rate also due to earthquakes from local to regional, with an accuracy sufficient to detect correctly many interesting phases in the records. Especially at local distances, these phases analyzed with the help of translational records from the same place, are expected to provide us with new information on the structure as well as the physics of seismic sources.

2 Basic principle of the sensor system

Assume point $\mathbf{x} + \delta\mathbf{x}$ situated close to point $\mathbf{x}$. The displacement $\mathbf{u}$ at such a point can be described by expanding displacement from $\mathbf{x}$ up to the first order as

$$\begin{aligned} u_i(\mathbf{x}+\delta\mathbf{x}) &= u_i(\mathbf{x}) + \frac{\partial u_i(\mathbf{x})}{\partial x_j}\delta x_j \\ &= u_i(\mathbf{x}) + \frac{1}{2}\left(\frac{\partial u_i}{\partial x_j} + \frac{\partial u_j}{\partial x_i}\right)\delta x_j \\ &\quad + \frac{1}{2}\left(\frac{\partial u_i}{\partial x_j} - \frac{\partial u_j}{\partial x_i}\right)\delta x_j \\ &= u_i(\mathbf{x}) + \epsilon_{ij}\delta x_j + \omega_{ij}\delta x_j, \end{aligned} \tag{1}$$

where u_i is the i-th component of the displacement vector $\mathbf{u}$, ϵ_{ij} is the symmetric strain tensor, and ω_{ij} is the anti-symmetric rotational tensor at point $\mathbf{x}$. In seismology, displacement (translation) is currently measured by seismographs and that strains can be determined by strainmeters. Up to the last decade, almost no attention was paid to rotational seismic motions.[1]

We have developed a device to determine the rotation of the seismic wavefield (Brokešová et al. 2009b; Brokešová and Málek 2010). More specifically, the device enables to measure the time derivative of rotation, i.e., the rotation rate $\mathbf{\Omega} = \mathrm{curl}\ \mathbf{v} = \mathrm{curl}\ \dot{\mathbf{u}}$, with $\mathbf{v}$ being particle velocity $\mathbf{v} = \dot{\mathbf{u}}$. Note that the rotation rate is analogous to the vorticity well-known from fluid dynamics.

Assume a right-handed Cartesian coordinate system with axes in east, north, and upward directions. More specifically, the first axis is horizontal and positive to the east, the second horizontal and positive to the north, and the third vertical and positive upward. In this coordinate system, we define two horizontal axis rotation rate components, Ω_1, Ω_2, and a vertical one, Ω_3, as

$$\begin{aligned} \Omega_1 &= \frac{1}{2}\left(\frac{\partial v_3}{\partial x_2} - \frac{\partial v_2}{\partial x_3}\right), \\ \Omega_2 &= \frac{1}{2}\left(\frac{\partial v_1}{\partial x_3} - \frac{\partial v_3}{\partial x_1}\right), \\ \Omega_3 &= \frac{1}{2}\left(\frac{\partial v_2}{\partial x_1} - \frac{\partial v_1}{\partial x_2}\right). \end{aligned} \tag{2}$$

Measurement of these quantities is based on determining the spatial derivatives of the ground velocity in Eq. 2, with those derivatives approximated by finite differences. This approach requires measuring the ground velocities at two points separated by a distance much smaller than the wavelength, but still large enough to allow differential sensing (i.e., the difference of the two records due to rotation). Sufficiently sensitive sensors, e.g., high gain geophones, have to be used to meet this requirement.[2]

The sensors are mounted in pairs on a rigid skeleton which is attached to the ground. They record the motion of this rigid skeleton. Due to the rigidity, the strain tensor in Eq. 1 vanishes, which means the equality of the corresponding spatial derivatives (the sign is opposite). Consequently, the rotation rate components of Eq. 2 simplify to

$$\begin{aligned} \Omega_1 &= \frac{\partial v_3}{\partial x_2} = -\frac{\partial v_2}{\partial x_3}, \\ \Omega_2 &= \frac{\partial v_1}{\partial x_3} = -\frac{\partial v_3}{\partial x_1}, \\ \Omega_3 &= \frac{\partial v_2}{\partial x_1} = -\frac{\partial v_1}{\partial x_2}. \end{aligned} \tag{3}$$

The shape of the skeleton is not important, except for its dimensions. Provided the dimensions of the skeleton are much smaller than the wavelength (by at least two orders), the rotation of the skeleton corresponds to the rotation of the ground at the center of the skeleton. Thanks to the skeleton's small dimensions, we can neglect

[1]This is so despite the fact that rotational motions contaminate translational records. The most significant effect is on horizontal accelerations contaminated by gravitation in the case of tilting of the accelerograph.

[2]The name geophone for the principal component of the system gave rise to the analogous name "Rotaphone" for the whole rotational sensor system.

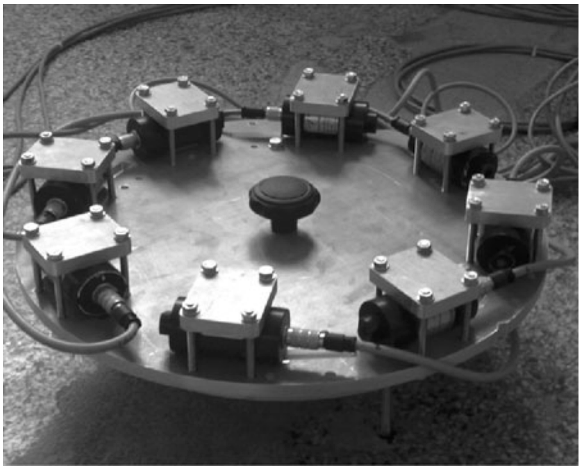

Fig. 1 A prototype of the new seismic rotational sensor system (Rotaphone) containing eight horizontal geophones (LF-24 made by Sensor Nederland b.v.) in four opposing pairs

the complex interaction of the rigid skeleton with the surrounding deformable continuum.

Figure 1 shows one prototype of our sensor system, only one of many possible realizations. The prototype contains eight horizontal geophones (LF-24 made by Sensor Nederland b.v.) arranged in four diametrical pairs. This prototype is intended to measure only the vertical rotation rate Ω_3 and two horizontal components of the ground translational velocity; it is an enhanced design of the sensor system described by Brokešová and Málek (2010).

Regardless of the various realizations of the measurement principle explained above, there are several important common features. Besides a small distance and rigid connection between individual sensors of the system, any rotation rate component must be determined using at least two diametrical sensor pairs. This is necessary to support the in situ calibration of the system described in the next section.

3 Calibration of individual elementary sensors

In the proposed method, the principal problem follows from the fact that the individual geophones in the sensor system are never exactly identical in their characteristics (transfer functions). This means that for the same input (ground, thence skeleton motion), they do not produce exactly the same output record. When the differential motions are to be determined, the distance between the sensors used must be small, which implies that also the difference between their recordings (the differential motion) will be small. Thus, small errors in records from each of the sensors caused by variations in sensor characteristics can lead to significant errors in the differential motion, so also in the measured seismic rotation rate. This is a serious problem with the potential to completely degrade the measurement of seismic rotation rates.

The way to overcome this problem is to calibrate the individual sensors precisely, at least relative to the paired sensors, implying the need to correct for their individual transfer functions. These transfer functions can be measured in the laboratory using a special calibration equipment; however, the precise transfer function may be sensitive to field conditions (temperature, atmospheric pressure, humidity, etc.) and may change with time (Ringler et al. 2010). It is, therefore, much better to calibrate the individual sensors in situ and simultaneously with each record of interest.

The presented method of the in situ calibration relies on the fact that the differential motions measured in our method are over-determined (two or more pairs for each rotation component). For example, when using the rotational sensor system in Fig. 1, four diametrical sensor pairs are used to derive the same differential motions that resolve a single rotation rate component (Ω_3). In the case of identical sensors, the recorded differences from all the pairs should be the same. In reality, they differ because the sensors in each pair are not identical. The in situ calibration must correct these differences.

For the sake of simplicity, let us consider two pairs of sensors of the same type (e.g., horizontal). We index the pairs by Roman numerals I and II (the generalization for additional pairs is straightforward). Let the true ground-motion time series to be recorded at the location of the sensors be $s_1^{\mathrm{I}}(t), s_2^{\mathrm{I}}(t)$ for one pair and $s_1^{\mathrm{II}}(t), s_2^{\mathrm{II}}(t)$ for the other pair. Here, the subscript distinguishes the two sensors in the given pair. Note that both these paired sensors record the same rotation rate component. We denote the corresponding complex Fourier spectra $S_1^{\mathrm{I}}(f)$, $S_2^{\mathrm{I}}(f)$, $S_1^{\mathrm{II}}(f)$, and $S_2^{\mathrm{II}}(f)$, where f stands for ordinary frequency and the actually recorded spectra by $R_1^{\mathrm{I}}(f)$, $R_2^{\mathrm{I}}(f)$, $R_1^{\mathrm{II}}(f)$, and $R_2^{\mathrm{II}}(f)$. The latter differ from the true ground-motion spectra according to

$$\begin{aligned} R_1^{\mathrm{I}}(f) &= S_1^{\mathrm{I}}(f)T_1^{\mathrm{I}}(f), \quad R_2^{\mathrm{I}}(f) = S_2^{\mathrm{I}}(f)T_2^{\mathrm{I}}(f), \\ R_1^{\mathrm{II}}(f) &= S_1^{\mathrm{II}}(f)T_1^{\mathrm{II}}(f), \quad R_2^{\mathrm{II}}(f) = S_2^{\mathrm{II}}(f)T_2^{\mathrm{II}}(f), \end{aligned} \tag{4}$$

where $T_1^{\mathrm{I}}(f)$, $T_2^{\mathrm{I}}(f)$, $T_1^{\mathrm{II}}(f)$, and $T_2^{\mathrm{II}}(f)$ are the frequency characteristics (transfer functions) of the individual sensors. The records from the individual sensors, $r_1^{\mathrm{I}}(t), r_2^{\mathrm{I}}(t), r_1^{\mathrm{II}}(t)$, and $r_2^{\mathrm{II}}(t)$, are inverse Fourier transforms of these complex spectra. As the sensors are presumably of the same type, we can assume that their frequency characteristics are similar. In the frequency domain, we can express the relation between $S_1^{\mathrm{I}}(f)$ and $S_2^{\mathrm{I}}(f)$ with the help of the measured $R_1^{\mathrm{I}}(f)$ and $R_2^{\mathrm{I}}(f)$ as

$$\frac{S_2^{\mathrm{I}}(f)}{S_1^{\mathrm{I}}(f)} = \frac{R_2^{\mathrm{I}}(f)}{R_1^{\mathrm{I}}(f)} t^{\mathrm{I}}(f), \tag{5}$$

where $t^{\mathrm{I}}(f) = T_1^{\mathrm{I}}(f)/T_2^{\mathrm{I}}(f)$ is a complex function nearly equal to unity. Analogously, we express

$$\frac{S_2^{\mathrm{II}}(f)}{S_1^{\mathrm{II}}(f)} = \frac{R_2^{\mathrm{II}}(f)}{R_1^{\mathrm{II}}(f)} t^{\mathrm{II}}(f), \quad \frac{S_1^{\mathrm{II}}(f)}{S_1^{\mathrm{I}}(f)} = \frac{R_1^{\mathrm{II}}(f)}{R_1^{\mathrm{I}}(f)} t^{\mathrm{II,I}}(f) \tag{6}$$

with the ratios $t^{\mathrm{II}}(f) = T_1^{\mathrm{II}}(f)/T_2^{\mathrm{II}}(f)$ and $t^{\mathrm{II,I}}(f) = T_1^{\mathrm{I}}(f)/T_1^{\mathrm{II}}(f)$ again close to complex unity.

Let us consider the differential motion between the sensors in pair I in the frequency domain, $S_1^{\mathrm{I}}(f) - S_2^{\mathrm{I}}(f)$. The corresponding finite difference may be used to approximate the spatial derivative

$$D(f) = \frac{S_1^{\mathrm{I}}(f) - S_2^{\mathrm{I}}(f)}{\Delta} = \frac{R_1^{\mathrm{I}}(f) - R_2^{\mathrm{I}}(f)t^{\mathrm{I}}(f)}{T_1^{\mathrm{I}}(f)\Delta}, \tag{7}$$

where Δ is the distance separating the sensors. If the sensor axes are perpendicular to the line connecting them, then the finite difference (7) also approximates the rotation rate component according to Eq. 8 in the paper by Brokešová and Málek (2010). Moreover, when measuring with the sensor system proposed in that paper, the same rotation must result from pair II, mounted on the same, nondeformable, skeleton. Thus,

$$D(f) = \frac{S_1^{\mathrm{II}}(f) - S_2^{\mathrm{II}}(f)}{\Delta} = \frac{R_1^{\mathrm{II}}(f) - R_2^{\mathrm{II}}(f)t^{\mathrm{II}}(f)}{T_1^{\mathrm{II}}(f)\Delta}. \tag{8}$$

The equality of Eqs. 7 and 8 yields the condition

$$\begin{aligned} &R_1^{\mathrm{I}}(f) - R_2^{\mathrm{I}}(f)t^{\mathrm{I}}(f) \\ &\quad = t^{\mathrm{II,I}}(f)(R_1^{\mathrm{II}}(f) - R_2^{\mathrm{II}}(f)t^{\mathrm{II}}(f)) \end{aligned} \tag{9}$$

The physical meaning of the expressions on either side of Eq. 9 is easy to interpret: In the frequency domain, Eq. 9 represents the true differential motion between the paired sensors multiplied by transfer function $T_1^{\mathrm{I}}(f)$ of a single sensor.

3.1 Full inversion

Equation 9 is valid for any frequency in the range in which the sensors provide reliable records. Thus, it represents a system of equations, one equation for each discrete frequency. The number of equations in the system is given by the number of samples used in the Fourier transform and is typically on the order of thousands. Three transfer function ratios: $t^{\mathrm{I}}(f)$, $t^{\mathrm{II}}(f)$, and $t^{\mathrm{II,I}}(f)$, are the unknowns in the system. It is usual to parametrize the transfer functions in a suitable way, so, for example, the parameters p_i can either be a scale factor plus poles and zeros or simply several discrete values in the frequency domain. The same parametrization can be applied for the transfer function ratios. For example, for any frequency of interest, $t^{\mathrm{I}}(f)$ is uniquely determined by these parameters

$$t^{\mathrm{I}}(f) = \phi(p_1, p_2, ...p_N;\ f), \tag{10}$$

with ϕ being a complex function (e.g., a set of interpolation polynomials or a rational function with poles and zeros) of N parameters, where N is usually not a very large number, say up to 20. We can parametrize the other two transfer function ratios similarly. In that case, Eq. 9 represents a system of thousands of equations (one equation for each sample frequency) for tens of unknowns (parameters of the transfer function ratios).

The problem of finding the unknowns is non-unique. Therefore, we introduce constraints to keep the transfer function ratios smooth and close to complex unity. These constrains are easily derived because we have sensors of the same type with very similar properties. This problem can be solved using general inverse methods (for an overview of the inverse methods, see Tarantola 1994). Specifically, we apply the new isometric inverse method (Málek et al. 2007) developed for weakly non-linear problems with many parameters. Our inverse problem is in this category. The starting parameter values are presumably close to the correct ones.[3] The isometric method postulates that the model space and data space are isometric. Isometry implies that the distance between two points preserves in both spaces. As all model–data vector pairs are used many times in successive iterations, the number of the forward problem computations is minimized. There is no necessity to deal with derivatives. The requirement for computer memory is therefore low. Details can be found in the paper by Málek et al. (2007).

The result of the inversion are the transfer function ratios $t^{\mathrm{I}}(f), t^{\mathrm{II}}(f)$, and $t^{\mathrm{II,I}}(f)$, which serve to correct the records $r_2^{\mathrm{I}}(t), r_1^{\mathrm{II}}(t)$, and $r_2^{\mathrm{II}}(t)$ with respect to the reference record $r_1^{\mathrm{I}}(t)$. From this process, we obtain corrected differential motions that are the same for pairs I and II. Both differences are influenced by transfer function $T_1^{\mathrm{I}}(f)$ so that the ground rotational motion can be obtained by correcting for $T_1^{\mathrm{I}}(f)$.

We illustrate the calibration technique described above on synthetic data with known rotation rate. Figure 2a shows simulated velocigrams from four horizontal geophones (A, B, C, D, oriented clockwise as viewed from above) comprising a Rotaphone. The four geophone records also contain the "input" synthetic rotation rate shown in Fig. 2b. Moreover, they have been altered by artificial differences in transfer functions. These differences are spectrally smooth and do not exceed 10% of the reference values (sensor A). Figure 2b also provides the average rotation rate obtained from the differential motions from the A–C and B–D geophone pairs (dotted line). The rotation rate calculated with our calibration technique (full inversion) is shown in Fig. 2b as the solid gray line. The original and calculated rotation rate curves are close both in waveform and in amplitude (they differ up to few percentage of peak input).

3.2 Simplified inversion

The calibration technique described above may be relatively numerically expensive for routine usage in the field with a small processor, especially when more sensor pairs are involved. For example, the laboratory example for the eight-sensor prototype (Fig. 1) required an inversion for 120 parameters. Thus, the method is not practical for processing copious data in a routine setting in a seismically active area. We have, therefore, developed and tested a simplified approach to the inverse problem described above to make it fast, effective, and simple to program. In this approach, we even do not need to introduce any parametrization for the transfer function ratios $t^{\mathrm{I}}(f), t^{\mathrm{II}}(f)$, and $t^{\mathrm{II,I}}(f)$ but only assume that they are smooth. The approach is further based on the assumption that (1) the result of inversion is much more sensitive to the ratios $t^{\mathrm{I}}(f)$ and $t^{\mathrm{II}}(f)$ of the transfer functions within the individual sensor pairs than to the "mixed" transfer function ratio $t^{\mathrm{II,I}}(f)$, and (2) the finite differences and corresponding rotation rate components are not very different from the starting model characterized by $t^{\mathrm{I}}(f), t^{\mathrm{II}}(f)$, and $t^{\mathrm{II,I}}(f)$ equal to complex unity (or, if available, values measured in the laboratory). With these starting values, we independently calculate the two sides of Eq. 9:

$$
\begin{aligned}
x_1(f) &= R_1^{\mathrm{I}}(f) - R_2^{\mathrm{I}}(f) t^{\mathrm{I}}(f), \\
x_2(f) &= t^{\mathrm{II,I}}(f)(R_1^{\mathrm{II}}(f) - R_2^{\mathrm{II}}(f) t^{\mathrm{II}}(f)).
\end{aligned} \tag{11}
$$

In the next step, we insert their average

$$
a(f) = (x_1(f) + x_2(f))/2 \tag{12}
$$

[3] They can be, if possible, measured in the laboratory. If such measured starting values are not available, complex units can be set as starting values instead.

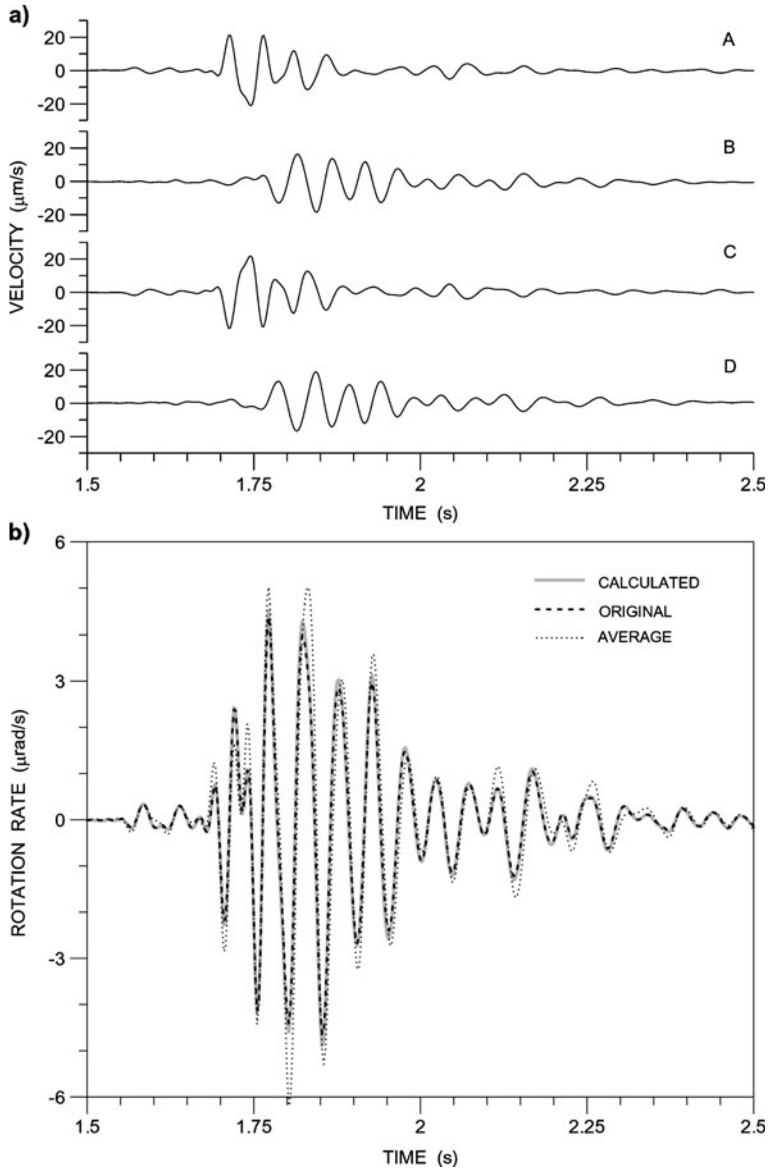

Fig. 2 Synthetic example using a full inversion: **a** four synthetic velocigrams simulating a four-sensor Rotaphone recording, including a theoretical rotation rates and the influence of sensor variability; **b** the original (theoretical) rotation rate (*dashed*) and the rotation rate calculated using our calibration technique (*gray solid*). For comparison, the figure also shows the average space derivative derived from the two sensor pairs of the four-sensor Rotaphone before calibration (*dotted*)

into Eq. 11 instead of $x_1(f)$ and $x_2(f)$. This yields new estimates of $t^{\mathrm{I}}(f)$ and $t^{\mathrm{II}}(f)$ keeping $t^{\mathrm{II,I}}(f)$ fixed at its initial value. The next step is smoothing of $t^{\mathrm{I}}(f)$ and $t^{\mathrm{II}}(f)$ and obtaining new $x_1(f)$ and $x_2(f)$ from Eq. 11. We again calculate their average, insert it into the left-hand sides of Eq. 11, and obtain new estimates of $t^{\mathrm{I}}(f)$ and $t^{\mathrm{II}}(f)$, iterating until the difference between $x_1(f)$ and $x_2(f)$, after each smoothing of the transfer function ratios, drops below a prescribed tolerance over the frequency range of interest. The main advantage of this approach is that it does not require any parameterization of transfer function ratios. Moreover, the "mixed" transfer function ratio is kept equal to its initial value and does not enter to the calculation. Consequently, the calculation is simpler than that of the full inversion, thus reduces computing time by a factor of ~60. We illustrate the simplified calibration technique and compare it to the full inversion method for the same synthetic example as in Fig. 2. Figure 3 shows the synthetic vertical axis rotation rate

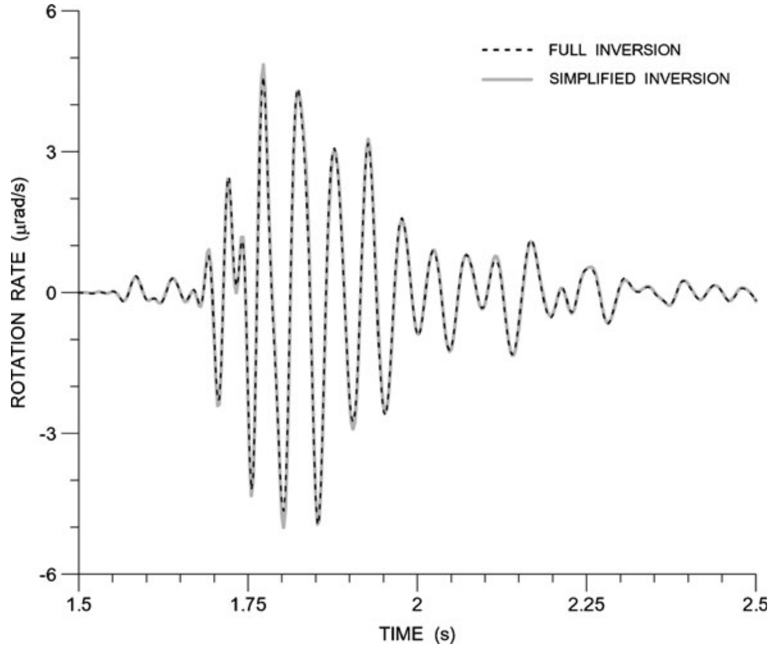

Fig. 3 Synthetic example of full and simplified inversion results: synthetic vertical axis rotation rate calculated using the full-inversion technique from Fig. 2 (*dashed*) is compared to the rotation rate calculated using our simplified calibration (*gray*)

calculated with the full inversion technique (dashed) and the rotation rate calculated by the simplified calibration (gray). The good match of the results is evident.

4 Laboratory calibration tests

We subjected our Rotaphone to elaborate testing at the Albuquerque Seismological Laboratory (ASL), US Geological Survey. ASL has excellent facilities to test seismic sensors, including rotational, over a wide frequency band. The laboratory measurements not only can be used to check instrument response to a pre-defined rotation (e.g., on a rotating table) but they can also provide valuable measurements of the frequency characteristics of the individual geophones and their mutual differences. These measured characteristics can be used to correct the data from the individual geophones prior to the in situ calibration. Thus, we start the inversion for Eq. 9 with starting values of the transfer function ratios much closer to reality than without such laboratory measurements.

To estimate the ratios between geophone transfer functions in each the four pairs of geophones (see Fig. 1), we used ambient Earth noise as a convenient wide-band input signal (we compute only spectral ratios between parallel geophones so they are insensitive to the spectrum of Earth noise input to geophones.) We recorded several hours of this ambient noise while periodically shifting the Rotaphone's azimuth by $\pi/4$ so that every pair twice occupied each azimuth. We then took the spectral ratio for a given pair of geophones, smoothed it for a sliding 4-s window, and averaged over all the azimuths to obtain a transfer function ratio for that pair insensitive to noise directionality. The results are four spectral ratios shown in Fig. 4, each smoothed over those hours and each representing the transfer function ratio between two geophones located on opposite sides of the Rotaphone, the pairs differenced to estimate the vertical axis rotation rate.

Figure 5 shows the settings for the laboratory experiment in which the Rotaphone was attached to a rotational shaking table. The Rotaphone was placed either in a center or off-center position, in Fig. 5, the off-center shift is 6 in. (15.24 cm). The motion of the table was a computer-controlled

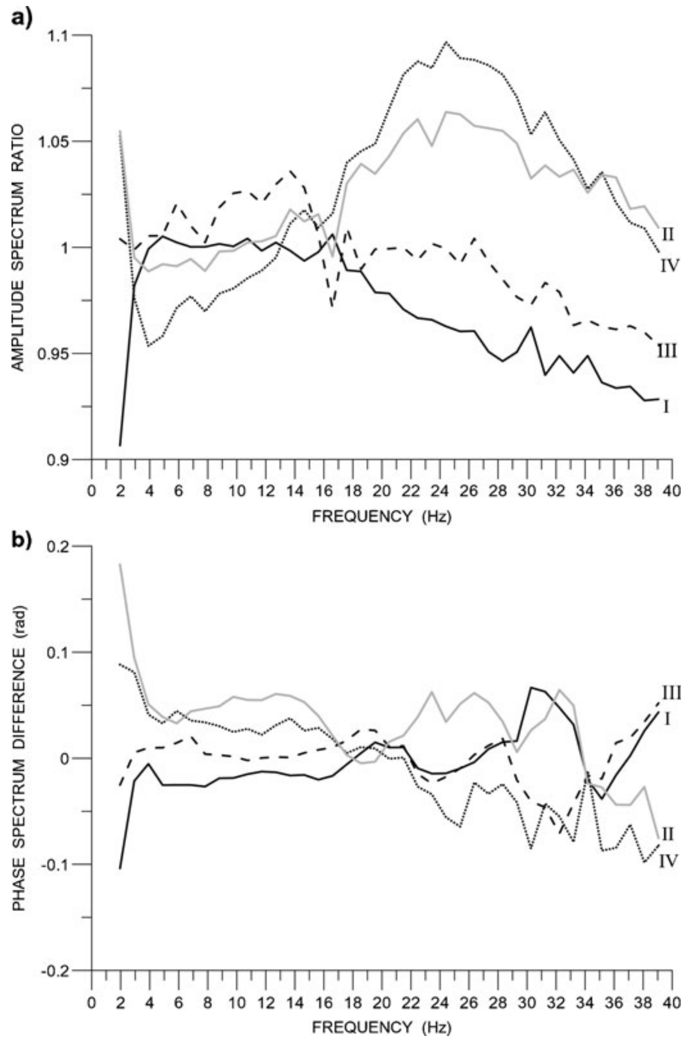

Fig. 4 **a** Amplitude ratios and **b** phase differences between the two individual geophones constituting each pair. These are mean spectral ratios for inputs of ambient Earth's noise

series of succeeding sine waves of different frequencies at a given amplitude level (a short example is shown in Fig. 6). Besides this harmonic shaking, a "random" motion of the table was made by hand. A fiber optic gyroscope (FOG; μFORS-1 Base Module, Northrop Grumman LITEF GmbH) is visible in Fig. 5 behind the Rotaphone; this FOG was the primary reference sensor.

Figure 6a shows an example of harmonic computer-controlled shaking at a frequency of 8 Hz and amplitude of 1.4 mrad/s with the Rotaphone shifted off-center by 3 in. (7.62 cm). The corresponding torsion (vertical axis rotation) rate measured by the reference FOG is shown as the dotted black line. The rotation rate measured by the Rotaphone is shown as the gray line. Thanks to this off-center shift, the Rotaphone is subjected not only to rotational but also to translational motion. In contrast to the rotation, for which we need to subtract the records from the geophones of a given pair, to obtain the translation at the center of the Rotaphone, we have to sum them (take the average). While for the rotation, after proper calibration, there is no difference between differential motions from each pair of geophones, for translation, we do obtain different values from different pairs since each pair measures translation in a different direction. For a given harmonic input, all the translational components must have

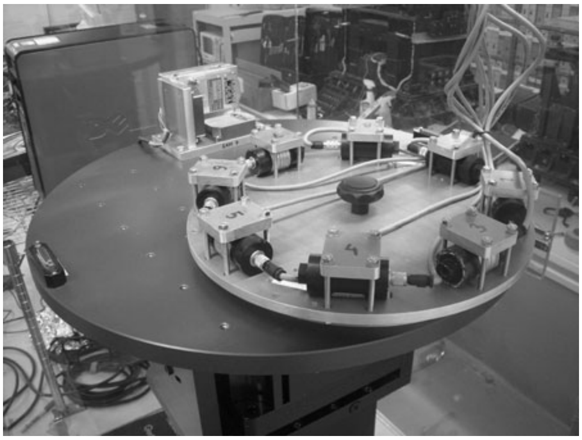

Fig. 5 Laboratory test on the vertical axis rotational shaking table: experimental setting with our eight-sensor Rotaphone (in off-center position) and reference fiber optic gyro (far edge)

the same frequency (8 Hz, in our case) as the rotation and must be in phase with it. The dotted line in Fig. 6b shows the tangential translational velocity at the Rotaphone center, 7.62 cm from the center of rotation. One of the geophone pairs (geophones 3 and 7, see Fig. 5) measured this component directly, and no projection into this tangential direction is necessary. This measured translation velocity can be compared to the instantaneous tangential velocity derived from rotation rate measured by the Rotaphone simply by multiplying by the off-center shift 7.62 cm. In absence of any other translational inputs, these two velocities must be identical, which is confirmed by Fig. 6b (the two results are within a line thickness of one another). This experiment is a good test of the Rotaphone measurements since each of the velocities in Fig. 6b is obtained by independent processing, the black dotted curve comes from summing the paired geophone records, and the gray curve comes from subtracting the data, and moreover, all the geophones contribute.

Figure 7 concerns an input motion produced by hand. In this way, we were able to achieve somewhat wider frequency band than for the monochromatic signal discussed above. In this experiment, the Rotaphone was mounted on the shaking table with an off-center shift of 6 in. (15.24 cm). Figure 7a compares the vertical rotation rates from the reference FOG (dotted black) and from the Rotaphone (gray). Both records are narrow band-pass filtered from 5 to 11 Hz to minimize the FOG noise (the FOG is not designed for such low amplitudes). Even so, noise remains, for example, at the beginning of the FOG time series before the significant motion starts. The noise contaminates the whole reference record, making comparisons difficult in some parts of the records. Therefore, we prefer Fig. 7b as more diagnostic. As with Fig. 6b, Fig. 7b compares the tangential

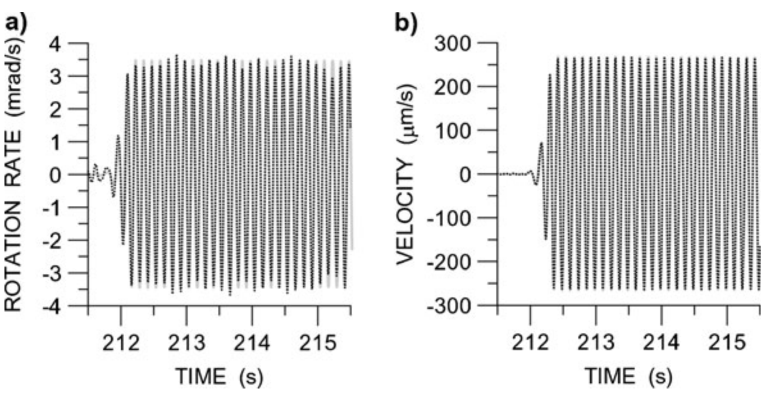

Fig. 6 Laboratory test on the vertical axis rotational shaking table: **a** comparison of the 8-Hz harmonic rotation signal measured by the Rotaphone (*gray*) and FOG (*dotted black*), **b** comparison of instantaneous, tangential, translational velocity of the Rotaphone (centered 7.62 cm from rotation axis) inferred by direct Rotaphone measurement (*dotted black*) or rotation rate and radius (*gray*)

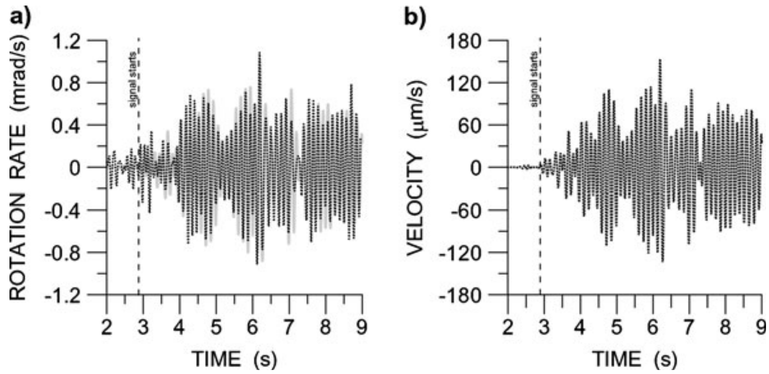

Fig. 7 Laboratory test on the vertical axis rotational shaking table for an input rotation signal produced by hand, measured **a** by the Rotaphone (*gray*) in the 15.24-cm off-center position (*black*) and by the reference FOG (*dotted black*), **b** comparison of instantaneous, tangential, translational velocity of the Rotaphone (centered 15.24 cm from rotation axis) inferred by direct Rotaphone measurement (*dotted black*) or rotation rate and radius (*gray*)

velocity of the Rotaphone center obtained from the measured angular velocity and known radius with the transverse velocity of that point obtained as the average of the least and most distant transverse geophones. Figure 7b shows an excellent match between these two quantities.

5 Rotation records from seismic sources

From May to June 2010, our seismic sensor (Rotaphone) was deployed at the station Nový Kostel (NKC) in West Bohemia (Czech Republic). The station is involved in the local seismic network WEBNET, operated jointly by the Institute of Geophysics and the Institute of Rock Structure and Mechanics, Czech Academy of Sciences, within the CzechGeo/EPOS project. The position of the station and the loci of the seismic events discussed below are shown in Fig. 8.

The region around Nový Kostel (and neighboring Vogtland region of Germany) is known for micro-earthquake swarm activity. The last important swarm occurred there at the end of 2008, but even during calm periods between swarms, isolated small shallow earthquakes occur. Measurements at station NKC have provided us with several rotational records from very local seismic events with $M_{\mathrm{L}} \leq 1$.

Figure 9 shows the small earthquake of 9 May 2010, 13:44:37 UTC. Its local magnitude was $M_{\mathrm{L}} =$ 0.3, epicentral distance 1.4 km (cf. Fig. 8), and depth 7.6 km. In Fig. 9, the vertical axis rotation rate (bottom) is shown with the two horizontal translational velocity components (transverse, middle; and radial, top), all recorded with the same Rotaphone. Note that the signal-to-noise ratio for this event is about 20. All the records here and below are filtered by a high-pass second-order Butterworth filter with a cut-off frequency of 2 Hz, the frequency above which the geophones used provide reliable records (have approximately flat transfer function). In Fig. 13a (discussed later), we see the filtered amplitude spectrum of the rotation rate (black) compared with the one of the transverse velocity component (gray) from this event. Note the higher-frequency content in the rotation rate compared to the translational velocity, which is related to the fact that rotation represents a derivative of translation.

In Fig. 9, we see that at the time of the P-wave onset in the radial component (2.07 s, see the dashed line), the rotation is negligible. Also the transverse component does not exceed the noise there. However, no later than about 180 ms after P onset, we see a rotation signal on the order of 10^{-7} rad/s. This signal derives from P-to-S conversion near the Earth's surface. This converted wave is visible also on the transverse component. This phase is relatively pronounced in both transverse and rotation components since the P wave is also relatively strong in comparison with the multiply

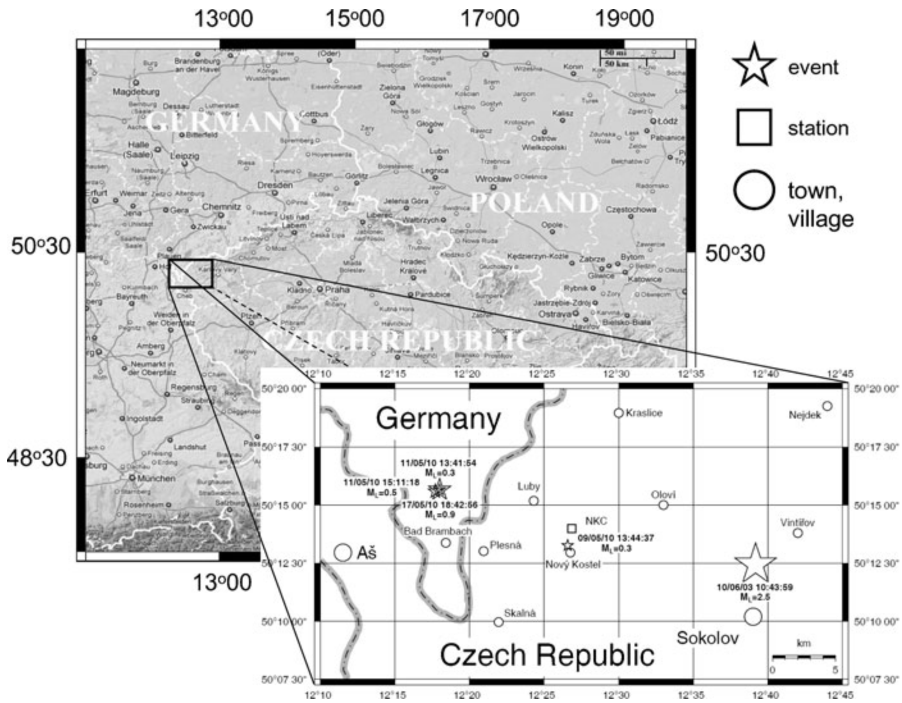

Fig. 8 Map of the West Bohemia/Vogtland seismically active region showing the position of the Nový Kostel station (NKC) and loci of the events discussed (*inset*) together with the broader geographic context

reflected and scattered P-waves in the following two seconds. The transverse and rotation components have multiply reflected and scattered P-to-S converted waves in this post-P time window. Another interesting feature is the S-to-P converted wave immediately before the S-wave onset. This wave converts to P near the Earth's surface and is seen in the radial component at 3.09 s (the second dashed line) but is visible neither in the transverse component nor in the vertical rotation rate at that time. The strongest rotational signal appears in the main S-wave group starting at about 3.15 s (the third dashed line). The maximum recorded amplitude of the vertical axis rotation rate is 2 μrad/s. The rotation rate maximum is later than the S-wave maximum in the horizontal translational components. The surface waves, which should also carry a substantial rotational signal, are not well developed because the source is almost 8 km deep and the instrument was close to the epicenter (1.4 km).

The next example is of several microearthquakes from the vicinity of Bad Brambach (Vogtland, close to the Czech-German border) recorded at station NKC in May 2010. Figure 10 shows seismograms of one small earthquake of 17 May 2010, 18:42:57 UTC, with a local magnitude of 0.9. The epicenter of this event is at a distance of 11 km and a depth of 10.5 km. Again, the figure shows the vertical axis rotation rate together with the radial and transverse translational velocities recorded by the geophones constituting the rotational sensor. Many features seen in Fig. 9 are present here too, including the near-surface S-to-P conversion preceding the S-waves (at about 4 s). One difference is that P onset and some of the P-to-S converted energy are masked by noise in Fig. 10. P and P-to-S weakness appears to be a manifestation of the radiation pattern. While in Fig. 9 P was relatively strong, the event in Fig. 10 is near the P-wave nodal plane. The scattered P waves on the radial and the scattered P-to-S conversions in the transverse and rotation components (about 1.5 s after the P-wave onset) are comparable to those seen in Fig. 9. A noticeable difference with respect to the event in Fig. 9 is a considerably larger time shift between the rotation rate maximum and the S-wave maxima in the horizontal translational velocity components. Surface waves are not seen for this event either because its epicentral distance is comparable to its depth.

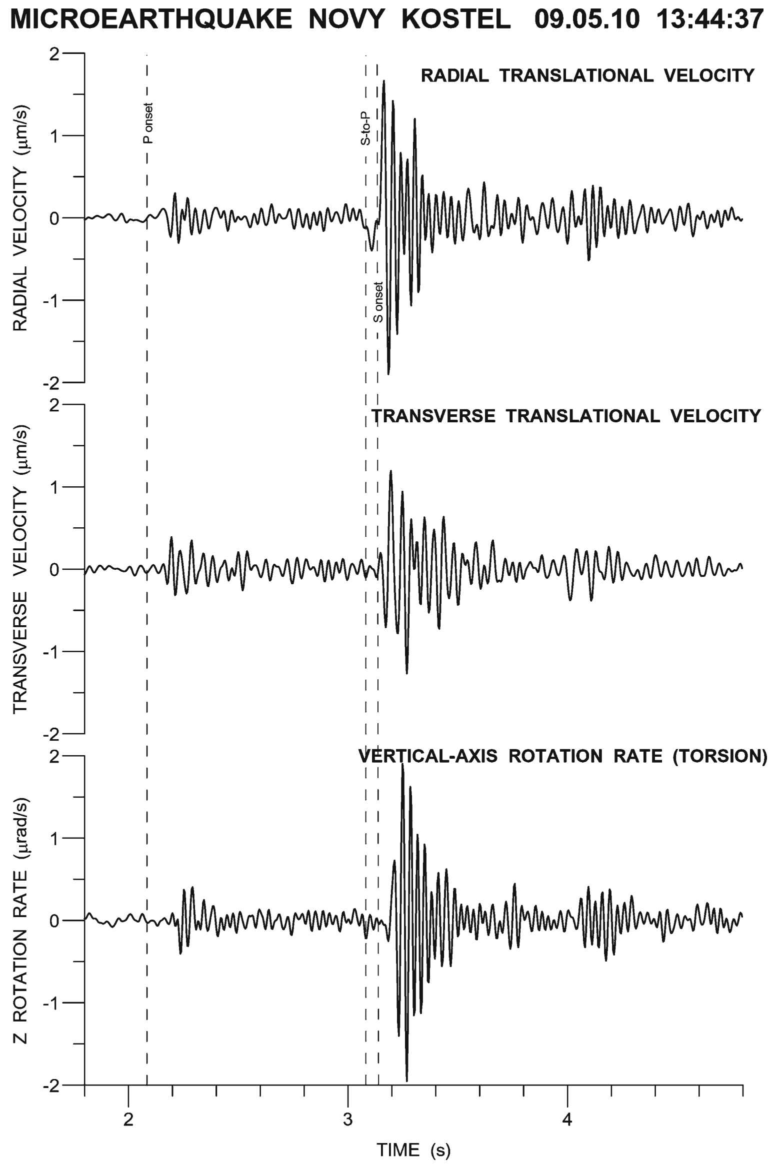

Fig. 9 Micro-earthquake near Nový Kostel, 9 May 2010, 13:44:37 UTC, $M_L = 0.3$, distance = 1.4 km, depth ~8 km. The radial and transverse translational velocity (*top* and *middle*) and the vertical axis rotation rate at the *bottom*

Figure 11 presents a detailed view of the S-wave group rotation rate from this and two other Bad Brambach earthquakes. The figure also provides the dates and local magnitudes of these events. Their foci are nearly identical at 11 km distance from the station. We assume that their mechanisms are very similar to one another, and a hypothesis is supported by the similarity in the S waveforms in Fig. 11. Note that while these three waveforms are very similar, they differ significantly from the waveform at the bottom of Fig. 9. Local magnitudes of these three events vary from 0.9 to 0.3, and rotation rates scale with magnitude, as expected, from 1.5 to 0.3 μrad/s (note that for the weakest event the signal-to-noise ration is about 2.5).

Figure 12 shows two translational and one rotational records as in Figs. 9 and 10 from a blast at Vintířov quarry, 15 km east of the station. The blast was on 3 July 2010, at 10:43:59 UTC, and its local magnitude was 2.5. Because the blast was fired at the Earth's surface, the waves propagated through very complex, shallow subsurface structures, so the records are qualitatively quite

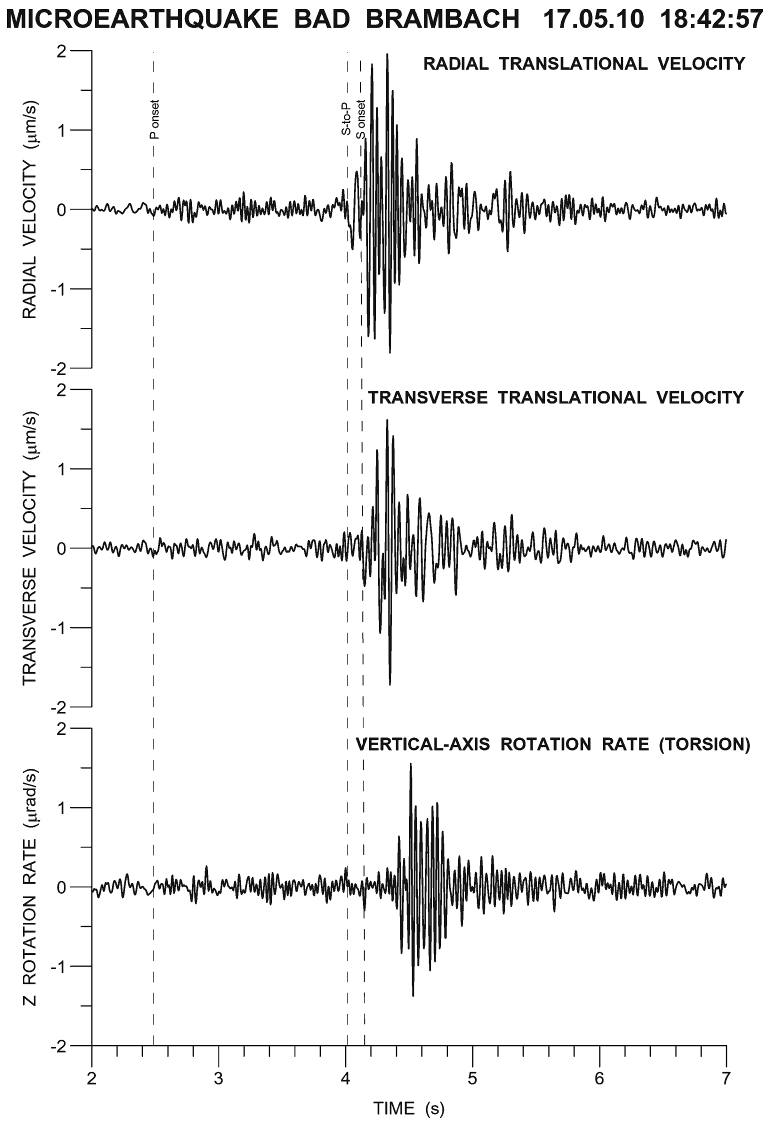

Fig. 10 Micro-earthquake near Bad Brambach, 17 May 2010, 18:42:57 UTC, $M_L = 0.9$, distance = 11 km, depth ~10 km. The radial and transverse translational velocity (*top* and *middle*) and the vertical axis rotation rate at the *bottom*

different from earthquake records in the previous figures. The P-wave onset is visible in the radial component (at about 3.4 s) but hidden by noise in the transverse and rotation records. This P-wave propagated as a diffracted wave through a structure with a strong subsurface velocity gradient (Málek et al. 2005) and is relatively weak since most of the energy propagated in the form of multiply reflected and scattered waves immediately beneath the surface. P is visible on all the seismograms from 4 s and obscures the arrival of diffracted S leaving its onset indistinct. The second dashed line at ~5.3 s corresponds to the theoretical S not as read from the seismograms. The Love wave onset appearing at the same time in the transverse component is also hidden by noise.

The Rayleigh wave in the radial component appears to arrive ~0.5 s later. Dispersion of the surface waves is apparent in both translational components; surface waves dominate the translational records. In contrast to previous figures, there is no distinctive maximum in the rotation rate record in Fig. 12. The rotation rate has noticeably higher-frequency content than the translational components.

Fig. 11 Vertical axis rotation rates due to three micro-earthquakes near Bad Brambach, May 2010, $M_L = 0.3 - -0.9$, distance = 11 km, depth ~10 km. Only main S-wave group is shown

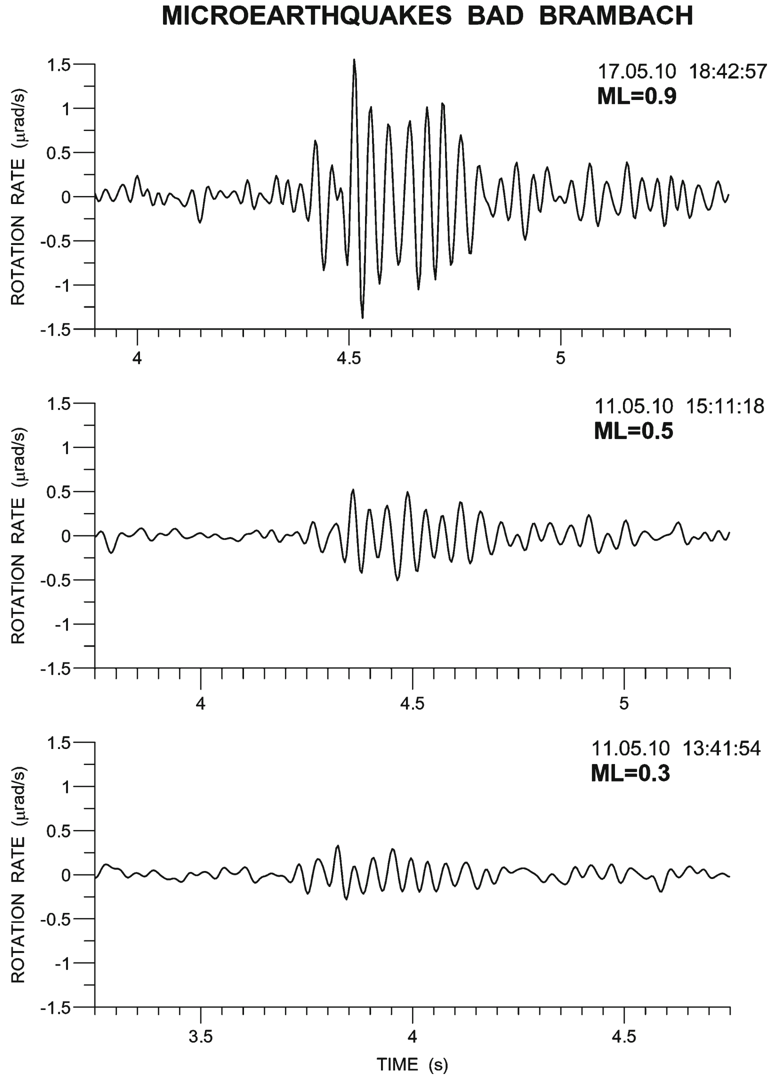

Figure 13 compares amplitude spectra of the largest event from each area: (a) the earthquake near Nový Kostel, $M_L = 0.3$, May 9, 13:44:37 UTC; (b) the earthquake near Bad Brambach, $M_L = 0.9$, May 17, 18:42:57 UTC; and (c) the quarry blast in Vintířov, $M_L = 2.5$, July 3, 10:43:59 UTC. The rotation rate spectra (black) are compared with the transverse velocity spectra (gray). Radial components are not shown because the transverse component is more relevant to rotation, as neither should contain P-wave contributions.

For all events in Fig. 13, the frequency content of vertical axis rotation rates is relatively higher than that of transverse ground velocities. This effect is the most pronounced for the blast record from Vintířov (Fig. 13c).

The rotation rate spectrum in Fig. 13a has two maxima: one around 20 Hz, the prevailing frequency of the ground velocity record,[4] and the other around 30 Hz. The rotation rate spectrum in Fig. 13b differs in shape, with the first maximum shifted a little to higher frequency (~24 Hz) and the second maximum (~30 Hz) considerably lower than in Fig. 13a. This contrast can be

[4]This prevailing frequency is very common for local earthquakes in the Nový Kostel area.

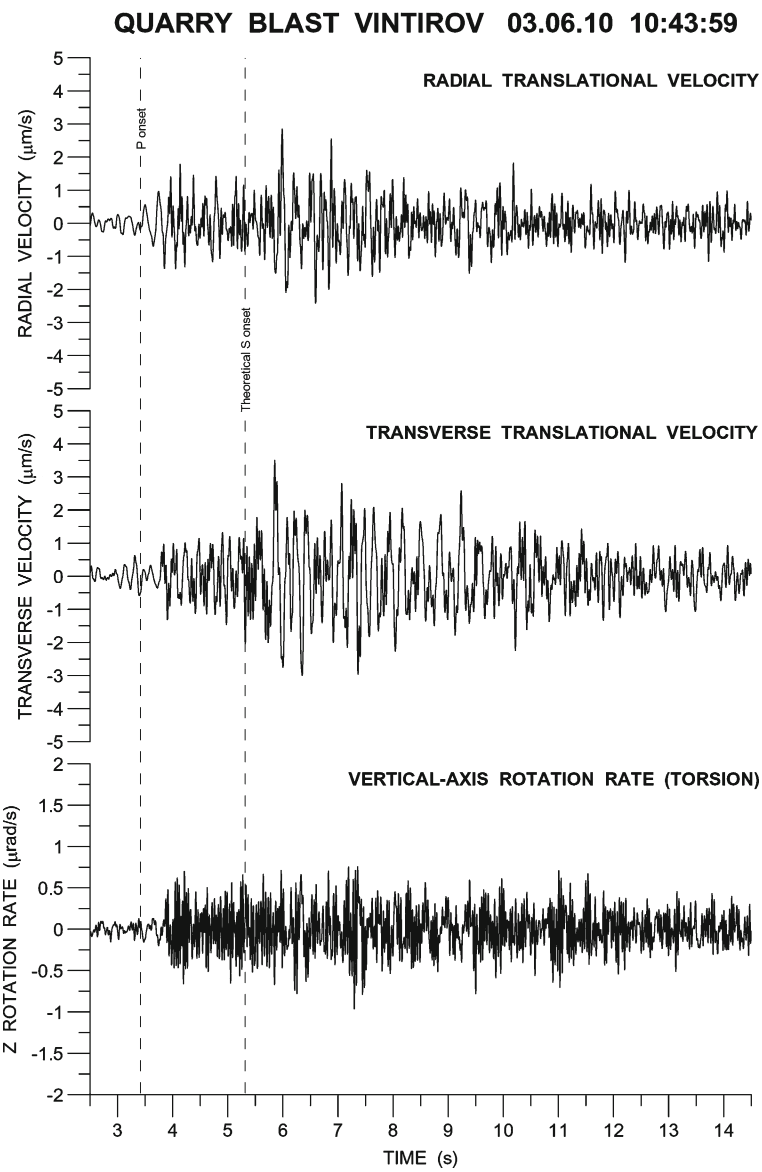

Fig. 12 Quarry blast near Vintířov, 3 June 2010, 10:43:59 UTC, $M_L = 2.5$, distance = 15 km, depth 0 km. The radial and transverse translational velocity (*top* and *middle*) and the vertical axis rotation rate at the *bottom*

explained as an attenuation effect since the hypocentral distance of the Bad Brambach event is about double that of the Nový Kostel event.

The spectral noise for the Vintířov blast (Fig. 13c) is just due to the fact that the spectrum was calculated from longer seismograms than in a and b. Nevertheless, overall shape of the rotation rate spectrum in Fig. 13c is similar to that in Fig. 13b. The two events have different source type (quarry blast compared to tectonic event). Moreover, the structure through which seismic waves propagate also differ considerably between the two events. For the Bad Brambach earthquake, most of the energy comes from depth and rays are nearly vertical at the Earth's surface because of a strong velocity gradient reported by Málek et al. (2004, 2005). The Vintířov blast energy largely propagates in the form of multiply reflected and scattered waves guided within complex near-surface layers. The only feature common to the two events is the source–receiver distance of about 15 km. We can only speculate that event hypocentral distance may have the primary influence on the shapes of the rotation rate

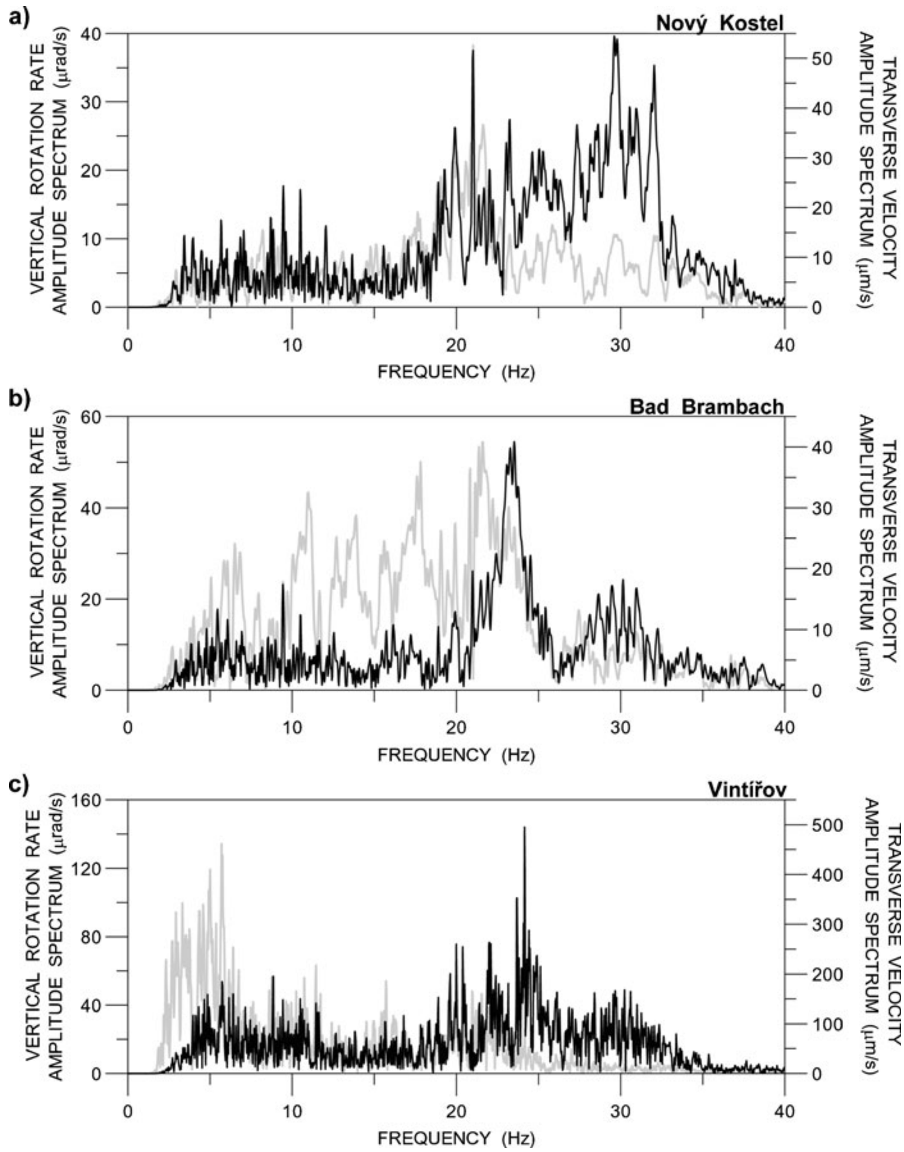

Fig. 13 Amplitude spectra for **a** the Nový Kostel event, 9 May 2010, 13:44:37 UTC, $M_{\mathrm{L}} = 0.3$; **b** the Bad Brambach event, 17 May 2010, 18:42:57 UTC, $M_{\mathrm{L}} = 0.9$; and **c** the Vintířov blast, 3 June 2010, 10:43:59 UTC, $M_{\mathrm{L}} = 2.5$. Vertical axis rotation rate amplitude spectra (*black*) are compared to the transverse translational velocity spectra (*gray*)

spectra. Confirming this inference would require systematic observations of many records.

6 Discussion, conclusions, and perspectives

We developed and tested a new rotational sensor, called a Rotaphone (an older prototype was described by Brokesova and Malek 2010). The Rotaphone sensor system consists of multiple geophones arranged in parallel pairs to allow measurement of differential motions and from these pairs to determine both translational velocities and rotation rates. The prototype presented in this paper is designed to measure the vertical axis rotation rate component (torsion). The Rotaphone operates in a high-frequency range, in this case above 2 Hz because we use 2-Hz geophones. A unique feature of the Rotaphone is its in situ calibration to correct for small differences in geophone characteristics. A major advantage of these instruments is their mobility and easy maintenance. They also achieve high sensitivity, up to a theoretical sensitivity limit of 10^{-8} rad/s.

However, this sensitivity can be achieved only in case of low instrumental and ambient Earth noise; we have reached 10^{-7} m rad/s to date. The device was originally developed for prospecting purposes. When it is used in combination with a repeating anthropogenic source, noise can be successfully suppressed by stacking, of course.

An important advantage of the Rotaphone is that it simultaneously measures translational velocity. These collocated measurements describe the wavefield in the vicinity of a station fully and can be used to distinguish the individual phases more reliably. For distant sources and long wavelengths, these collocated rotation and translation records can be used also to retrieve the phase velocity and propagation direction from single-station measurement (Igel et al. 2007) and to sharpen tomographic images (Bernauer et al. 2009). Rotaphone measurements offer rotation and translation records with the same transfer functions, which makes their joint usage easier.

Laboratory testing at the Albuquerque Seismological Laboratory, USGS provided absolute and relative transfer functions between geophone pairs (including corrections for skeleton rigidity). These corrections precede our in situ calibration and provide the starting values of the transfer function ratios very close to the correct ones. The tested prototype correctly measured the rotation rate produced by the ASL rotational shaking table, but the tests were restricted to a minimum amplitude of 10^{-4} rad/s, four orders higher than the theoretical sensitivity limit of our Rotaphone and a few orders higher than the rotations caused by small ($M_{\mathrm{L}} \leq 1$) local earthquakes (e.g., the West Bohemia seismoactive area). To verify Rotaphone data for such week events, it is necessary to compare its output to an independent rotational measurement in the high-frequency range (above 2 Hz). The authors plan such tests for the very near future.

The rotating shaking table produces, of course, very little translation in contrast to real ground motions, which are dominated by translation. To characterize the significance of rotation, let us introduce the rotation to translation ratio (RTR) expressed in radians per meter. In our case, it relates vertical axis rotation rate peak amplitude to horizontal translational velocity peak amplitude (derived from its radial and transverse components). In the laboratory experiments, the RTR was 6.56 rad/m during measurements with an off-center shift of 15.24 cm (the radius of the Rotaphone is 15 cm) and 13.12 rad/m during measurements with an off-center shift of 7.62 cm.

We deployed the Rotaphone at the existing Nový Kostel seismic station, West Bohemia, Czech Republic. We recorded rotation rates due to both natural (micro-earthquakes) and anthropogenic (quarry blast) seismic sources at epicentral distances from 1.5 to 15 km. Local magnitudes ranged from 0.3 to 2.5. The measured rotation rates are of the order of 10^{-6} rad/s for the local earthquakes to 10^{-7} rad/s for the blast.

The RTR values for the seismic events in Figs. 9, 10, and 12 are given in Table 1, together with peak translational velocities and peak vertical axis rotation rates. The largest RTR value was detected for the nearest Nový Kostel event from Fig. 9; its focus is situated almost directly beneath the station. For the Bad Brambach event in Fig. 10 at almost twice as large hypocentral distance, the RTR is significantly smaller. The blast from Vintířov, at about the same distance from the station at the Bad Brambach event, has an extremely small RTR, about 20% of that of the Nový Kostel event, suggesting that for local events, the RTR factor depends on hypocentral distance, source

Table 1 The maximum vertical rotation rate amplitude Ω_3 in comparison to the maximum horizontal translational velocity $v^H = \sqrt{(v^R)^2 + (v^T)^2}$ derived from radial and transverse components. Note that all these quantities refer to particle motion in the horizontal plane. The RTR (Rotation to Translation Ratio) is the ratio Ω_3/v^H

Event	Ω_3 (μrad/s)	v^H (μm/s)	RTR (rad/m)
Nový Kostel ($M_{\mathrm{L}} = 0.3$; May 9, 13:44:37)	2.0	2.0	1.0
Bad Brambach ($M_{\mathrm{L}} = 0.9$; May 17, 18:42:57)	1.6	2.5	0.6
Vintířov ($M_{\mathrm{L}} = 2.5$; Jul 3, 10:43:59)	0.9	3.8	0.2

type, and probably on radiation pattern and geological structure along the wavepaths. More systematic investigation of additional field records is necessary.

A new tri-axial Rotaphone prototype, a 6DOF sensor, is being developed. The basic principle of this new device is the same as that explained here, but the skeleton is of a different shape to allow the geophones to be arranged both in horizontal and vertical planes. In the near future, we plan to apply these 6DOF instruments to investigating induced seismicity in the salt works of Provadia, Bulgaria and in a systematic study of rotational seismic motions in the West Bohemia/Vogtland region.

Acknowledgements The authors would like to thank John R. Evans and Charles R. Hutt for experimental assistance during testing and for providing reference fiber optic gyro data. This work was supported by the Czech Science Foundation, project no. P210/10/0925. Field measurements were carried out at the WEBNET station supported by the CzechGeo/EPOS project.

References

Bernauer M, Fichtner A, Igel H (2009) Inferring earth structure from combined measurements of rotational and translational ground motions. Geophysics 74:WCD41–WCD47. doi:10.1190/1.3211110

Brokešová J, Málek J (2010) New portable sensor system for rotational seismic motion measurements. Rev Sci Instrum 81. doi:10.1063/1.3463271

Brokešová J, Málek J, Štrunc J (2009a) Generator of rotational seismic waves, rotational seismic sensor system and seismic measuring set. Patent CZ 301218

Brokešová J, Málek J, Štrunc J (2009b) Rotational seismic sensor system, generator of rotational seismic waves and seismic measuring set. Patent CZ 301217

Huang BS (2003) Ground rotational motions of the 1999 Chi-Chi, Taiwan earthquake as inferred from dense array observations. Geophys Res Lett 30:1307–1310. doi:10.1029/2002GL015157

Igel H, Schreiber U, Flaws A, Schuberth B, Velikoseltsev A, Cochard A. (2005) Rotational motions induced by the M8.1 Tokachi-oki earthquake, September 25, 2003. Geophys Res Lett 32. doi:10.1029/2004GL022336

Igel H, Cochard A, Wassermann J, Flaws A, Schreiber U, Velikoseltsev A, Pham ND (2007) Broad-band observations of earthquake-induced rotational ground motions. Geophys J Int 168:182–196. doi:10.1111/doi:j.1365-246X.2006.03146.x

Lee WHK, Huang BS, Langston CA, Lin CJ, Liu CC, Shin TC, Teng TL, Wu CF (2009) Progress in rotational ground-motion observations from explosions and local earthquakes in Taiwan. Bull Seismic Soc Am 99:958–967. doi:10.1785/0120080205

Lin CJ, Liu CC, Lee WHK (2009) Recording rotational and translational ground motions of two TAIGER explosions in northeastern Taiwan on 4 March 2008. Bull Seismic Soc Am 99:1237–1250. doi:10.1785/0120080176

Málek J, Janský J, Novotný O, Rossler D (2004) Vertically inhomogeneous models of the upper crustal structure in the West Bohemian seismoactive region inferred from the CELEBRATION 2000 refraction data. Stud Geophys Geod 48:709–730. doi:10.1023/B:SGEG.0000045478.42945.6a

Málek J, Horálek J, Janský J (2005) One-dimensional qP-wave velocity model of the upper crust for the West Bohemia/Vogtland earthquake swarm region. Stud Geophys Geod 49:501–524. doi:10.1007/s11200-005-0024-2

Málek J, Růžek B, Kolář P (2007) Isometric method: efficient tool for solving non-linear inverse problems. Stud Geophys Geod 51:469–490. doi:10.1007/s11200-007-0028-1

Moriya T, Teisseyre R (2006) Design of rotation seismometer and non-linear behaviour of rotation components of earthquakes. In: Teisseyre R, Takeo M, Majewski E (eds) Earthquake source asymmetry, structural media and rotation effects. Springer, Berlin, pp 439–450

Nigbor RL (1994) Six-degree-of freedom ground-motion measurement. Bull Seismic Soc Am 84:1665–1669

Nigbor RL, Evans JR, Hutt CR (2009) Laboratory and field testing of commercial rotational seismometers. Bull Seismic Soc Am 99:1215–1227. doi:10.1785/0120080247

Ringler AT, Gee LS, Hutt CR, McNamara DE (2010) Temporal variations in global seismic station ambient noise power levels. Seismol Res Let 81:605–613. doi:10.1785/gssrl.81.4.605

Schreiber U, Klügel T, Stedman GE (2003) Earth tide and tilt detection by a ring laser gyroscope. J Geophys Res 108. doi:10.1029/2001JB000569

Schreiber U, Velikoseltsev A, Rorthacher M, Klügel T, Stedman GE, Wiltshire DL (2004) Direct measurement of diurnal polar motion by ring laser gyroscopes. J Geophys Res 109. doi:10.1029/2003JB002803

Schreiber U, Hautmann JN, Velikoseltsev A, Wassermann J, Igel H, Otero J, Vernon F, Wells JPR (2009) Ring laser measurements of ground rotations for seismology. Bull Seismic Soc Am 99:1190–1198. doi:10.1785/0120080171

Stedman GE (1997) Ring laser tests of fundamental physics and geophysics. Rep Progr Phys 60:615–688

Takeo M (1998) Ground rotational motions recorded in near-source region of earthquakes. Geophys Res Lett 25:789–792

Tarantola A (1994) Inverse problem theory, methods for data fitting and model parameter estimation. Elsevier, Amsterdam

Teisseyre R, Takeo M, Majewski E (eds) (2006) Earthquake source asymmetry, structural media and rotation effects. Springer, Berlin